Journal of Applied Polymer Science

Magnetic Polymeric Nanoparticles Functionalized by Mannose-Rhodamine Conjugate for Detection of *E. coli*

Samon Trungkathan,[1] Duangporn Polpanich,[2] Srung Smanmoo,[3] Pramuan Tangboriboonrat[1]

[1]Department of Chemistry, Faculty of Science, Mahidol University, Bangkok 10400, Thailand

[2]National Nanotechnology Center (NANOTEC), Thailand Science Park, Klong Luang, Pathumthani 12120, Thailand

[3]National Center for Genetic Engineering and Biotechnology (BIOTEC), Thailand Science Park, Klong Luang, Pathumthani 12120, Thailand

Correspondence to: P. Tangboriboonrat (E-mail: pramuan.tan@mahidol.ac.th)

ABSTRACT: Mannose-rhodamine (Rh) conjugate (80% yield) was synthesized in a one-pot reaction and immobilized onto magnetic polymeric nanoparticles (MPNP; 43% magnetic content) of poly(styrene/divinyl benzene/acrylic acid). The resulting nanoparticles contained MPNP as a substrate, mannose as an *E. coli* receptor and Rh as a fluorescent signaling unit. TEM imaging clearly demonstrated that multiple mannose-Rh MPNPs could be captured by *E. coli* strain ORN178. The fluorescent signal from captured nanoparticles was emitted at 580 nm. These results indicate that mannose-Rh MPNP offers a simple and rapid strategy for bacterial detection. © 2013 Wiley Periodicals, Inc. J. Appl. Polym. Sci. **2014**, *131*, 40012.

KEYWORDS: adsorption; *E. coli* detection; fluorescence; non-polymeric materials and composites; polystyrene

Received 15 June 2013; accepted 27 September 2013

DOI: 10.1002/app.40012

INTRODUCTION

Escherichia coli (*E. coli*) is pathogenic bacteria which can cause intestinal and extra-intestinal infections, e.g., diarrhoea, food poisoning, and urinary tract infections.[1,2] Therefore, the detection of *E. coli* is necessary for maintaining food safety and hygiene. Currently available methods for detection of *E. coli* are mainly based on cell culture and colony counting techniques which are tedious and time intensive.[3–5] Alternative techniques with high selectivity and sensitivity using the polymerase chain reaction (PCR) and enzyme-linked immunosorbent assays (ELISA) have been developed.[5] However, these techniques require long detection times, complicated procedures, enrichment prior to analysis, and expensive apparatus.[6,7] Hence, a new technique, which is rapid, reliable, simple, specific, and sensitive for the detection of *E. coli*, is highly desirable.

Detection of *E. coli* based on the carbohydrate–protein interaction has been of great interest due to the fact that infection and colonization of *E. coli* strains is mediated by the interaction between mannose on the host cell surface and the FimH protein of *E. coli*.[8,9] The weakness of mannose–FimH interaction requires the attachment of a single *E. coli* cell to several mannose molecules for efficient complex formation. Magnetic nanoparticles (MNPs) with a high surface/volume ratio or large contact area containing mannose groups can be used as a substitute for host cells and aid in the detection of *E. coli*.[10,11] The large contact area on the MNPs is predicted to enhance the interaction between *E. coli* and mannose allowing for separation of *E. coli* from the surrounding material when an external magnetic field is applied. Magnetic glycol-nanoparticles (MGNPs), prepared by functionalization of silica-coated magnetite with D-mannose, have been previously used for the determination of *E. coli* with a detection limit of 10^4 cells/mL. However, a major drawback of this technique is the multi-step procedure for preparation of MGNPs followed by staining of *E. coli* cells in the MGNPs/*E. coli* complexes with a fluorescent dye (PicoGreen) prior to detection using epifluorescent microscopy.[12,13] To eliminate the staining step, fluorescent MNP composed of a magnetic core coated or embedded with fluorophores has been proposed. In addition, a protective layer or spacer between the MNP core and fluorophore is required in order to suppress the quenching of fluorophore by MNP. The low molecular weight chitosan (CS) covalently bound to fluorescein isothiocyanate (FITC) was synthesized and then immobilized onto MNPs. However, the fluorescent intensity of the FITC-labeled CS coated MNP was low, presumably due to the quenching effects due to the short chain length of the CS spacer.[14] Attempts to reduce MNP mediated quenching have utilized magnetic polymeric nanoparticle (MPNP) or MNPs encapsulated in a polymer matrix. MPNPs have the additional advantages of being easily functionalized for immobilizing of fluorescent dyes or targeting ligands and the oxidation and leakage of magnetite are

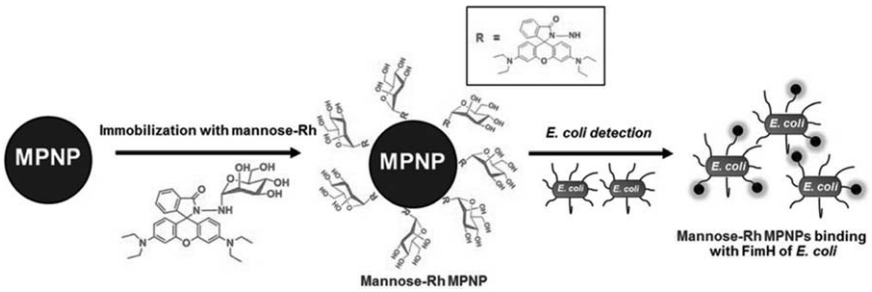

Scheme 1. MPNP functionalized by mannose-Rh molecules for *E. coli* detection.

prevented. Recently, MNPs embedded into poly(styrene/divinyl benzene/acrylic acid) (PS/DVB/AA) have been synthesized via the miniemulsion polymerization process.[15] These MPNPs contained a high magnetic content (53%) and were coated with high molecular weight CS prior to immobilization with FITC for cell-labeling applications. The high molecular weight CS was an effective spacer between the MPNP and FITC and prevented the electron transfer process that causes fluorescent quenching.[16] Although FITC provides a strong emission intensity with pH-dependency and a simple labeling process, its poor photostability reduces its utility.[17] Rhodamine B (Rh B) and its derivatives have received much interest as alternatives to FITC due to their long absorption and emission wavelengths, high fluorescence quantum yields, large extinction coefficient and good photostability.[18–20]

The goal of the present study was to develop a mannose-Rh based *E. coli* detection system with PS/DVB/AA MPNP as a substrate. Mannose is predicted to act as an *E. coli* receptor and Rh as a fluorescent signalling unit. The mannose-Rh molecules were synthesized and immobilized onto the surface of MPNP for *E. coli* detection as shown in Scheme 1. The mannose-Rh conjugate was synthesized via the coupling reaction between mannose and Rh hydrazide using $Y(OTf)_3$ as Lewis acid catalyst. To understand interaction involved in the attachment of the fluorescent signaling unit to MPNP substrate, Rh B, a precursor for synthesis of mannose-Rh conjugate, coated onto PS/DVB/AA MPNP was first examined. The driving force for the interaction between the MPNP and Rh B is an electrostatic interaction between negatively charged MPNP and positively charged Rh B molecule.[21] The synthesized mannose-Rh conjugate was subsequently produced and bound to MPNP via a hydrophobic interaction.[22,23] The deposition of Rh B or mannose-Rh onto MPNPs was monitored using UV–vis spectroscopy. The binding between mannose-Rh MPNPs with *E. coli* cell was investigated with TEM and the fluorescence properties of mannose-Rh MPNPs upon binding to *E. coli* were also determined.

EXPERIMENTAL

Materials

Styrene (St; Sigma Aldrich, Purum) and acrylic acid (AA; Aldrich, Purum) monomers were purified by passing through a column packed with neutral aluminium oxide and basic aluminium oxide (Fluka, Purum) before being distilled under reduced pressure. D-(+)-mannose (Sigma), aniline (Sigma-Aldrich), yttrium(III) triflate [$Y(OTf)_3$] (Fluka), rhodamine B (Sigma), hydrazine monohydrate (Fluka), iron (III) chloride ($FeCl_3$; Riedel-deHaën), iron (II) chloride tetrahydrate ($FeCl_2{\cdot}4H_2O$; Sigma Aldrich, Purum), 25% ammonium hydroxide (NH_4OH) solution (Merck, AR), oleic acid (OA; Fluka, Natural from suet), divinyl benzene (DVB; Merck, Synthese), hexadecane (HD; Fluka, Purum), sodium dodecyl sulfate (SDS; Sigma, GC) and potassium persulphate (KPS; Fluka, Puriss) were used as received. Deionized water was used throughout the work. *E. coli* ORN178 and ORN208 strains, kindly provided by Professor P.E. Orndroff, North Carolina State University, United States, were grown in sterile Luria-Bertani (LB) media. A single colony of each strain was lifted from an agar plate and inoculated in LB media (10 mL) and grown overnight to approximately 10^9 cfu/mL. Cells were washed thrice by centrifugation (9,000 rpm, 5 min; Tomy, MX-301) with phosphate buffered saline (PBS; 1×, pH 7.4) prior to use.

Synthesis of Mannose-Rh Conjugate

Rh hydrazide was prepared by mixing Rh B with hydrazine monohydrate in dry ethanol and refluxed with stirring under N_2 for 24 h.[24] After cooling to RT, brine was added to the reaction mixture before extraction with dichloromethane three times. The combined organic layers were dried over anhydrous magnesium sulphate and the filtrate was concentrated to give Rh hydrazide as a brown solid. Rh hydrazide (457 mg, 1.00 mmol) was then dissolved in anhydrous methanol (10 mL) while stirring at RT under a N_2 atmosphere. D-Mannose (180 mg, 1.00 mmol) and $Y(OTf)_3$ (0.1 mmol) were subsequently added into the Rh hydrazide solution and the mixture was allowed to stir at RT for 24 h. After completion, the mixture was concentrated and the crude product was purified using column chromatography (CH_2Cl_2/MeOH, 9 : 1, v/v) resulting in the isolation of the mannose-Rh conjugate as a pink solid. Percent yield of mannose-Rh conjugate was gravimetrically determined (80%). ^{1}H-NMR (400 Hz, DMSO) δ 7.77 (*m*, 1H), 7.49 (*m*, 2H), 6.99 (*m*, 1H), 6.64 (*d*, $J = 8.9$ Hz, 1H), 6.32 (*m*, 5H), 6.21 (*d*, $J = 8.7$ Hz, 1H), 5.59 (*d*, $J = 10.7$ Hz, 1H), 4.80 (*d*, $J = 5.2$ Hz, 1H), 4.63 (*m*, 2H), 4.03 (*m*, 1H), 3.50 (*m*, 1H), 3.41 (*m*, 1H), 3.22 (*m*, 2H), 2.83 (*m*, 1H), 2.37 (*m*, 1H), 1.08 (*m*, 12H). ^{13}C-NMR (500 Hz, DMSO) δ 12.47, 43.67, 61.14, 64.60, 66.84, 69.64, 74.40, 78.01, 86.04, 97.29, 105.17, 105.55, 107.76, 108.11, 122.26, 123.42, 127.78, 128.18, 128.93, 132.58, 148.07, 151.96, 152.39, 152.89, 164.77. HRMS (ESI^+) found: 619.3126 $(M + H)^+$, calcd for $C_{34}H_{43}N_4O_7$ 619.3053.

Synthesis of MPNPs

MNP was prepared by the co-precipitation method as previously described.[15] In this process, an excess of NH_4OH solution was added into a mixture of an aqueous solution of $FeCl_3$ and $FeCl_2{\cdot}4H_2O$ (molar ratio 2 : 1) under N_2 atmosphere while stirring at RT. The prepared MNPs (7.0 g) were then coated with OA (1.5 mL). After removal of excess OA by washing with methanol, the OA coated MNPs (OA-MNPs) were redispersed into a mixture of St (1.5 g), DVB (1.0 g), AA (0.045 g), and HD (0.3 g). The mixture was poured into an aqueous solution of SDS (0.072 g) and deionized water (24.0 g) for preparation of MPNP via miniemulsion polymerization. At 72°C, an aqueous solution of KPS (0.1 g) in deionized water (2.0 g) was added to start the polymerization. The reaction was incubated for 22 h with continuous stirring under N_2 and the resulting MPNPs were centrifuged (5,000 rpm, 30 min; Hettich, Universal 320) before characterization.

Preparation of Rh B-MPNPs

Rh B-MPNPs were prepared by adding Rh B (0.02 g/mL, 0.1 mL) into MPNPs (0.1% w/v, 10 mL) followed by incubation with shaking at RT for 12 h. The obtained Rh B-MPNPs were separated by applying a magnet and the supernatant was carefully removed by pipetting. Particles were washed and redispersed in deionized water. Two cycles of magnetically induced separation, washing, and redispersion were performed. All supernatant solutions were collected and analyzed by UV–vis spectroscopy (JASCO, V-530) to determine the amount of Rh B present on MPNPs.

Preparation of Mannose-Rh MPNPs

The synthesized mannose-Rh (50 mg, 0.08 mmol) was dissolved in dichloromethane (10 mL) prior to addition of MPNPs (5 mg) and deionized water (20 mL). The mixture was ultrasonicated (Vibracell, VCX 500) in an ice bath at 60% amplitude for 10 min. The resulting suspension was stirred overnight at RT to evaporate dichloromethane and was subsequently centrifuged (12,000 rpm, 20 min). The mannose-Rh functionalized MPNPs were washed twice with deionized water and the supernatant containing unbound mannose-Rh was collected for UV–Vis measurement to calculate the amount of mannose-Rh conjugate onto MPNPs.

Characterizations of OA-MNPs, MPNPs, Rh B-MPNPs, and Mannose-Rh MPNPs

X-ray Powder Diffraction (XRD). The crystallographic structure of the OA-MNPs was investigated by XRD (Rigaku TTRAX III, 18 kW) with a high power Cu $K\alpha$ X-ray source. The phases of sample were identified through the Power Diffraction File (PDF) database (JCPDS, International centre for Diffraction Data). The average crystallite size of MNPs was calculated from the Debye–Scherrer equation,[25]

$$D = \frac{0.9\lambda}{\beta\cos\theta} \quad (1)$$

where D is average crystallite size (Å), λ is an X-ray wavelength (Cu $K\alpha$: $\lambda = 1.5418$ Å), β is the full width at half maximum (FWHM; in radians), and θ is the Bragg diffraction angle.

Transmission Electron Microscopy (TEM). The morphology of OA-MNPs and MPNPs and selected area electron diffraction (SAED) pattern of the OA-MNPs were observed using TEM (FEI, TECNAI G^2). A few drop of dilute sample was placed on a carbon-coated copper grid. The sample was dried overnight at room temperature before investigation.

Thermogravimetric Analysis (TGA). TGA (Metter Toledo, SDTA851) was employed to determine the magnetic content of MPNP. The measurement was performed from 40 to 600°C under N_2 with a heating rate of 20°C/min.

Fourier Transform Infrared Spectroscopy (FTIR). The chemical structure and functional groups of MPNPs were examined by FTIR (Perkin Elmer, SpectrumGX). Samples were dried at 80°C and compressed with KBr. Spectra were recorded twice using 16 scan and a resolution of 4 cm^{-1}.

Zeta Potential and Particle Size Measurement. The hydrodynamic diameter and zeta potential of MPNPs and Rh B-MPNPs were measured by using a zeta sizer (Malvern, Nano ZS) at 25°C. For determination of zeta potentials, the pH of sample was adjusted by addition of 0.01*M* HCl or NaOH. Each sample was repeatedly measured in triplicate.

UV–Vis Spectrophotometry and Fluorescence Spectrofluorometry. The UV–vis spectra of MPNPs, Rh B-MPNPs and mannose-Rh MPNPs dispersed in methanol (1%v/v) and Rh B and mannose-Rh conjugate dissolved in methanol (1%v/v) were recorded on UV–vis spectrophotometer using a quartz cell of 1.0 cm path length. To determine the amount of Rh B and mannose-Rh conjugate onto surface of MPNPs, UV–vis measurement of supernatant solutions obtained from Rh B-MPNPs and mannose-Rh MPNPs preparations were also conducted as mentioned before.

The fluorescence properties of MPNPs and Rh B-MPNPs were investigated using a spectrofluorometer (JASCO, FP-6200). Fluorescence emission spectra were obtained by exciting the samples at 553 nm.

Detection of *E. coli* Employing Mannose-Rh MPNPs

To determine the effectiveness of mannose-Rh MPNPs in detecting *E. coli* two different bacterial strains, ORN178 and ORN208 were tested. Strain ORN178 contains the FimH protein that specifically binds to mannose, whereas ORN208 does not express FimH and fails to bind to mannose and should not interact with mannose-Rh MPNPs. Growth of *E. coli* cells was conducted according to reported procedures.[10] Mannose-Rh MPNPs (2 mg/mL) were added to *E. coli* in PBS buffer (10^9 cfu/mL) with stirring and after incubation for 1 h at RT with gentle shaking, the samples were exposed to a magnet. The supernatant was carefully removed by pipetting and the nanoparticles were washed three times before re-suspending with PBS to the original volume. The binding between mannose-Rh MPNPs and *E. coli* was investigated using TEM after dropping a small amount of the mannose-Rh MPNPs/*E. coli* suspension (10 μL) onto a carbon-coated copper grid. A drop of phosphotungustic acid (1% w/v) was used to negatively stain the specimen for 1 min. Fluorescence of mannose-Rh MPNPs

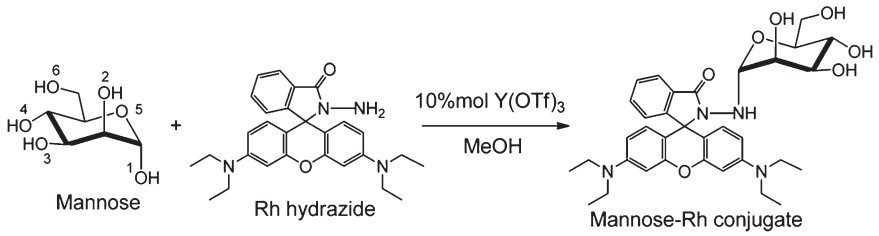

Scheme 2. Synthesis of mannose-Rh conjugate.

binding with *E. coli* was measured using a microplate reader (Molecular devices, SpectraMax M2). The emission spectrum of mannose-Rh MPNPs/*E. coli* cells was measured with an excitation wavelength at 556 nm.

RESULTS AND DISCUSSION

Synthesis of Mannose-Rh Conjugate

A simple one-pot procedure was used for the synthesis of mannose-Rh conjugate (Scheme 2). The mannose-Rh conjugate was simply prepared from a coupling reaction between mannose and Rh hydrazide by using $Y(OTf)_3$ as a catalyst and resulted in a good yield of product (80%). With $Y(OTf)_3$ catalysis, the hydroxyl group of mannose was activated which produces a good leaving group. The corresponding *N*-glycosylated product was then obtained via the formation of oxocarbenium, promoted by the elimination of an activated hydroxyl group at the anomeric carbon, followed by the nucleophilic addition from the Rh nitrogen. The structure of the mannose-Rh conjugate was examined by ^{1}H-NMR, ^{13}C-NMR, and mass spectrometry. The ^{1}H-NMR spectra of mannose, Rh hydrazide, and mannose-Rh conjugate were presented in Figure 1(A–C). The ^{1}H-NMR spectrum of mannose-Rh conjugate in Figure 1(C) exhibited peaks at 6.21, 6.32, and 6.64 ppm indicative of the xanthene protons of Rh hydrazide in Figure 1(B). Aromatic protons peaks for Rh hydrazide appeared at 6.99, 7.49, and 7.77 ppm, whereas peaks at 2.37, 2.83, 3.22, 3.41, 3.50, 4.03, 4.63, and 4.80 ppm in Figure 1(C) corresponded to mannose protons in Figure 1(A). In addition, ^{1}H-NMR of the mannose-Rh conjugate showed N–H proton at 5.59 ppm indicating the conjugation of rhodamine hydrazide and mannose moiety. For the ^{13}C-NMR spectrum of mannose-Rh conjugate, the peaks at 86.04, 105.17, 105.55, 107.76, 108.11, 122.26, 123.42, 127.78, 128.18, 128.93, 132.58, 148.07, 151.96, 152.39, and 152.89 were characteristic peaks for Rh hydrazide, while the peaks at 61.14, 64.60, 66.84, 69.64, 78.01, and 97.29 were those of mannose. Mass spectra analysis revealed a peak at $m/z = 619.3126$ $(M + H)^+$ which corresponded to molecular mass of the mannose-Rh conjugate. These spectroscopic data confirmed the presence of the mannose-Rh conjugate.

Characterization of OA-MNPs and MPNPs

The crystallographic structure of OA-MNPs was demonstrated by the XRD pattern as shown in Figure 2(A). The position and relative intensity of the peaks at 220, 311, 400, 511, and 440 indicated the crystalline characteristic of Fe_3O_4 (magnetite).[15,26] The average particle size of 5 nm, calculated by using the Debye–Scherrer equation, was similar to that determined from TEM image as shown in Figure 2(B). In addition, distinct rings, characteristics of polycrystalline samples of SAED, are observed in Figure 2(C). These results illustrate the good crystalline nature of the Fe_3O_4 nanoparticles.[27]

As already mentioned, MPNP was used as a substrate for immobilization of mannose-Rh conjugate due to (1) its high specific surface area for attaching mannose-Rh molecules; and (2) the ease of removing *E. coli* cells using a magnet. The OA-MNPs (dark spots) were then embedded in a PS/DVB/AA matrix (light phase) as seen in the TEM micrograph in Figure 3(A). The uniform distribution of MNPs in each spherical MPNP, having an average size of 202 ± 14 nm, in the absence of non-magnetic nanoparticles was clearly observed. It is possible that the presence of DVB, a crosslinking agent of PS, increased the internal viscosity of MPNP during polymerization preventing MNPs from moving outward. Previous studies have demonstrated the formation of non-magnetic nanoparticles and inhomogeneous distribution of MNPs within MPNP in the absence of DVB.[15]

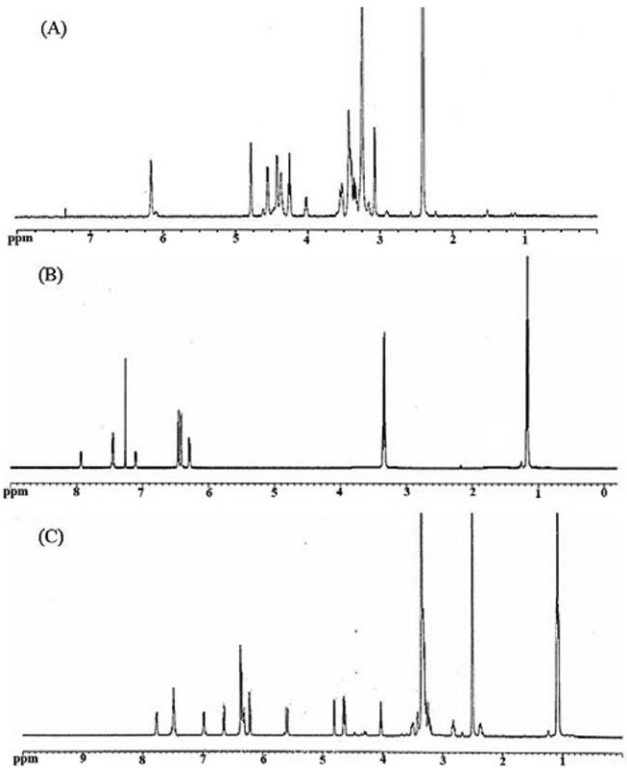

Figure 1. ^{1}H-NMR of (A) mannose, (B) Rh hydrazide, and (C) mannose-Rh conjugate.

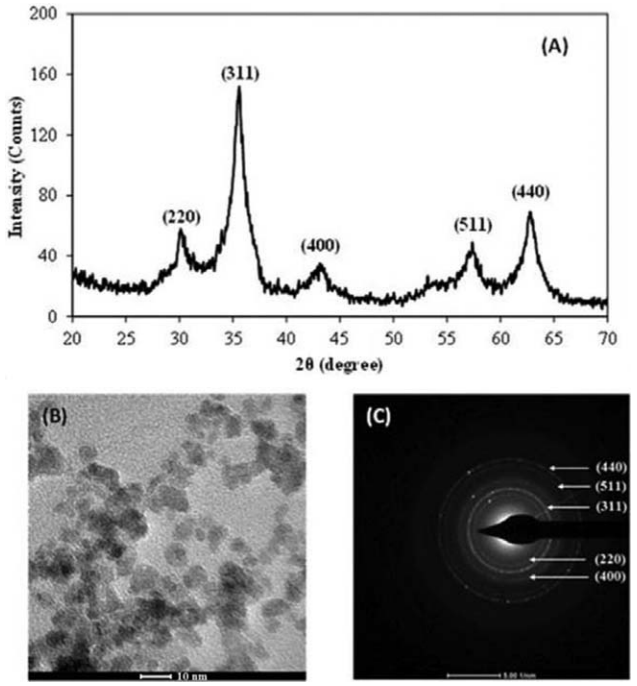

Figure 2. (A) XRD pattern, (B) TEM micrograph, and (C) SAED of the OA-MNPs.

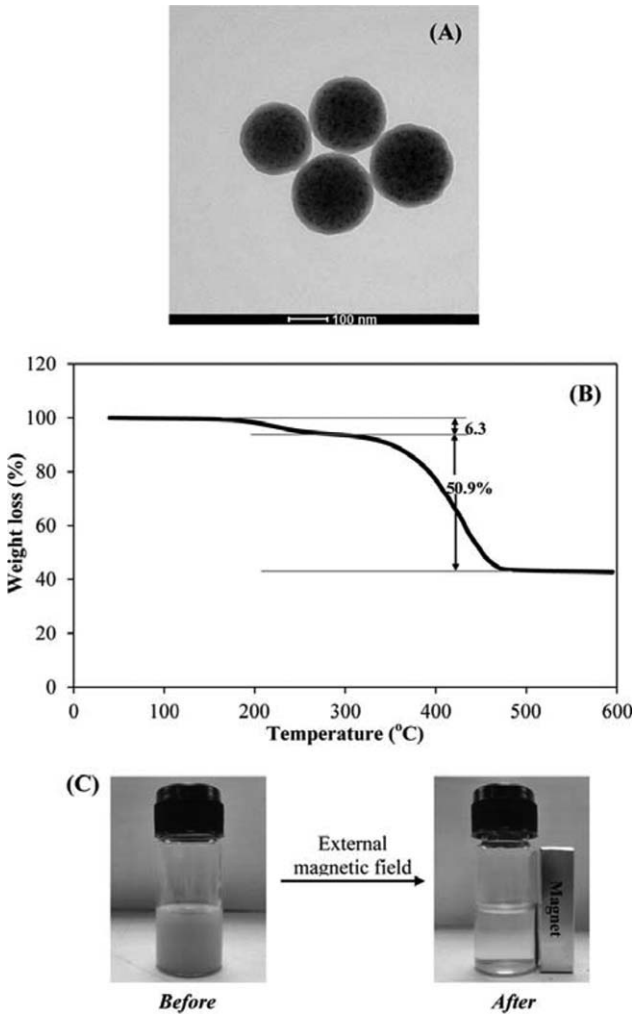

Figure 3. (A) TEM micrograph of MPNPs, (B) TGA thermogram of MPNPs, and (C) photographic images of MPNPs before and after applying a magnet.

The Fe_3O_4 content was determined by TGA and the thermogram is presented in Figure 3(B). The weight loss of MPNPs was divided into two steps. The first step of 6.3% between 100 and 300°C was ascribed to the dehydration and decomposition of residual surfactant and hexadecane.[15,28] The second step of 50.9% between 300 and 500°C was caused by the decomposition of the polymer matrix.[29] It was concluded from the residual weight loss that the magnetic content of the MPNPs was 42.8%. Due to the high magnetic content complete magnetic separation of MPNPs (10% v/v) was achieved within 3 min when a magnet was applied, as shown in Figure 3(C). The magnetic separation capability of the MPNPs provided for the effective separation of target molecules bound to MPNPs.

The chemical structure and functional groups of MPNPs were analyzed by FTIR (Figure 4). The existence of AA was indicated by the peak at 1707 cm^{-1} relating to the C=O stretching of carboxyl group.[16] In addition to peaks for C-H stretching (aromatic stretching vibration at 3060 and 3026 cm^{-1}, C–H stretching vibration at 2924 and 2853 cm^{-1}), three absorption peaks at 1602, 1493 and 1453 cm^{-1} were consistent with the vibration of C–C bonds in benzene ring and confirmed the presence of PS and DVB. Moreover, the double peaks at 760 and 700 cm^{-1} corresponded to the out-of-plane bending vibration of C–H groups in the monosubstituted benzene ring. The presence of the *p*-substituted benzene of DVB was also supported by observation of aromatic C–H in-plane bending at 989 and 905 cm^{-1} and out-of-plane bending at 797, 760, and 700 cm^{-1}. The peak between 450 and 620 cm^{-1} was assigned to the stretching vibration for the Fe–O bond of Fe_3O_4.[30–32]

Characterization of Rh B-MPNPs and mannose-Rh MPNPs

The presence of Rh B on the MPNP surface was verified using zeta potential measurements. Figure 5 shows the zeta potentials of MPNPs and Rh B-MPNPs as a function of pH. The negative zeta potential values of MPNPs at all pHs in curve 5A were due to the carboxyl groups of AA and sulfate groups of the added SDS.[33] After coating MPNPs with Rh B, the absolute zeta potentials of Rh B-MPNPs were lower than those of MPNPs as shown in curve 5B. It appears that the presence of Rh B shielded the negative charge of the exposed AA or shifted the shear plane around the MPNPs.[21,34]

To confirm the attachment of Rh B onto MPNP, UV-vis spectroscopy was also employed and the spectra of Rh B, MPNPs and Rh B-MPNPs are displayed in Figure 6.

The curve 6C shows a maximum absorbance peak at 555 nm for Rh B-MPNPs which is similar to that for Rh B in curve 6A. However, a peak at 555 nm was not observed in curve 6B for MPNPs, indicating that this peak was diagnostic for the presence of Rh B. These results confirmed the successful deposition

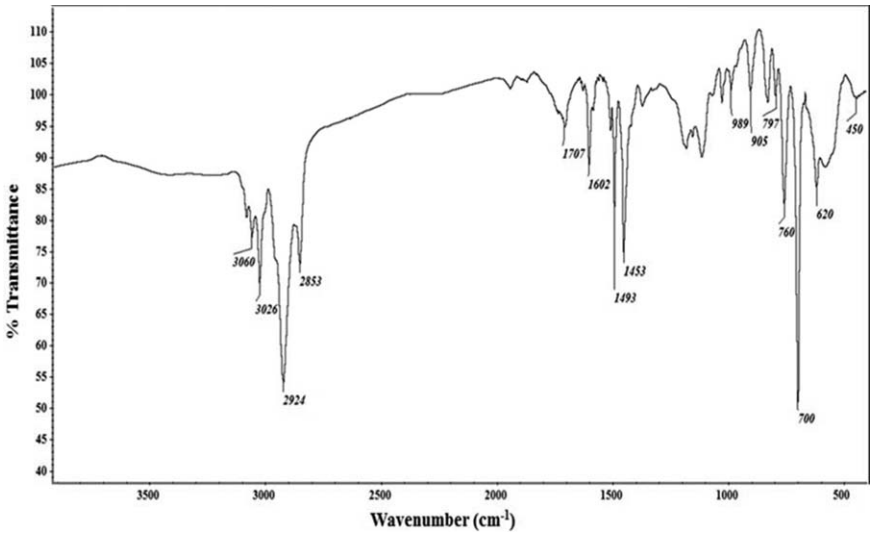

Figure 4. FTIR spectrum of MPNPs.

of Rh B onto MPNPs. The amount of Rh B deposited onto MPNPs (10 mg) was 376 μg or 37.6 mg/g of MPNPs, based on the concentration of Rh B in the supernatant, 1624 µg, calculated from absorbance peak of Rh B at 553 nm.

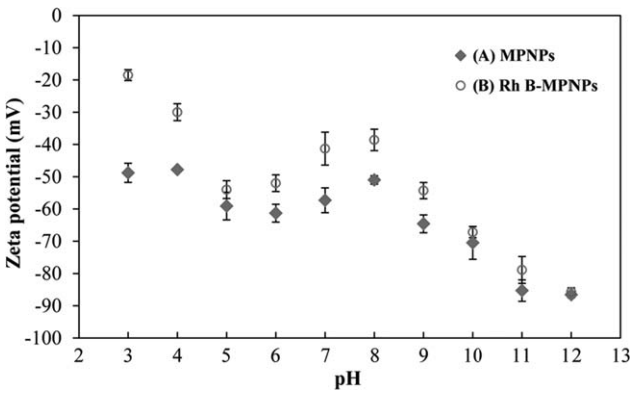

Figure 5. Zeta potentials of (A) MPNPs and (B) Rh B-MPNPs as a function of pH.

The fluorescence properties of Rh B, MPNPs and Rh B-MPNPs were examined by spectrofluorometer and the fluorescence emission spectra at 550–620 nm are presented in Figure 7.

When excited at 553 nm, the Rh B solution exhibited an emission at 572 nm (curve 7A). The fluorescence spectrum of MPNPs in curve 7B did not display a fluorescence peak within this range, while the emission maximum of Rh B-MPNPs in curve 7C was at 574 nm. This also indicated that Rh B was deposited onto MPNPs.

Since mannose-Rh molecules were prepared from the reaction of mannose with Rh hydrazide, the mannose-Rh could attach onto MPNP through the hydrophobic interaction.[22,23] It was expected that the Rh portion would be anchored on the surface of MPNP, while the mannose was exposed to the water phase and available for binding with FimH protein on *E. coli* cells.

Using UV–vis spectrophotometry the presence of mannose-Rh onto MPNP was further confirmed. The UV–vis spectra of

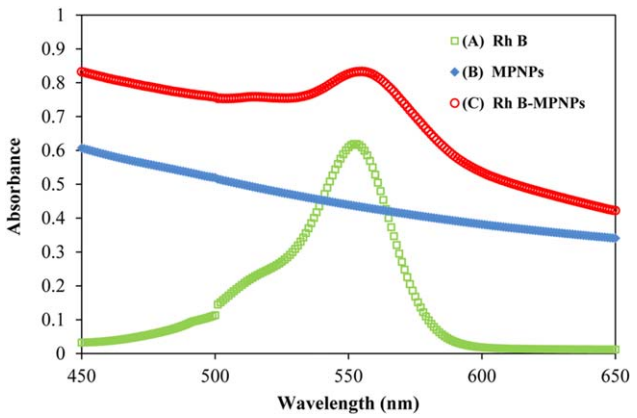

Figure 6. UV–vis spectra of (A) Rh B, (B) MPNPs, and (C) Rh B-MPNPs. [Color figure can be viewed in the online issue, which is available at wileyonlinelibrary.com.]

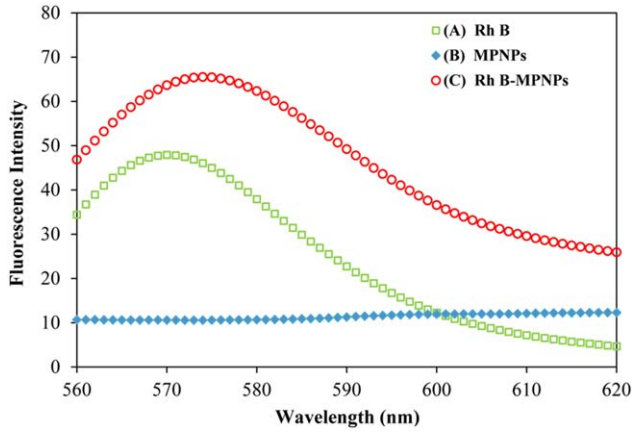

Figure 7. Fluorescence emission spectra of (A) Rh B, (B) MPNPs, and (C) Rh B-MPNPs. [Color figure can be viewed in the online issue, which is available at wileyonlinelibrary.com.]

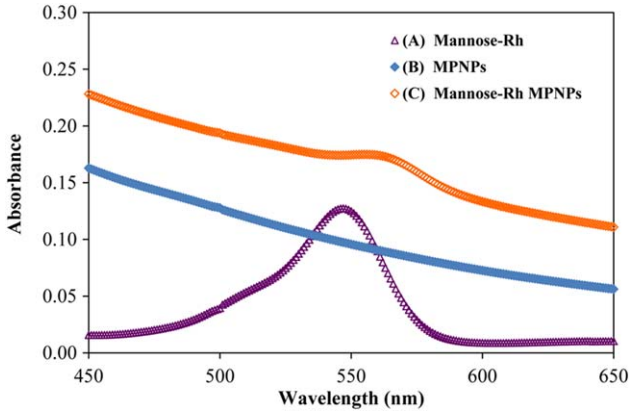

Figure 8. UV–vis spectra of (A) mannose-Rh, (B) MPNPs, and (C) mannose-Rh MPNPs. [Color figure can be viewed in the online issue, which is available at wileyonlinelibrary.com.]

mannose-Rh, MPNPs and mannose-Rh MPNPs are shown in Figure 8.

The spectrum of mannose-Rh in curve 8A displays an absorbance peak at 556 nm that is absent in curve 8B for MPNPs. When mannose-Rh was immobilized onto MPNP, the maximum absorption peak was red shifted at 567 nm (curve 8C). This confirmed that MPNP was modified by mannose-Rh.

Similar to the case of Rh B-MPNP, the amount of mannose-Rh adsorbed onto MPNP was determined from the analysis of the UV–vis absorption of the supernatant at 556 nm. The results indicated that the amount of free mannose-Rh was 49.75 mg and, hence, that amount of mannose-Rh attached onto MPNP was 0.25 mg or 50 mg/g of MPNP. It was possible that several mannose-Rh molecules could attach to the surface of MPNP resulting in enhanced binding between mannose on the MPNPs and FimH protein of *E. coli*.[12,13,35]

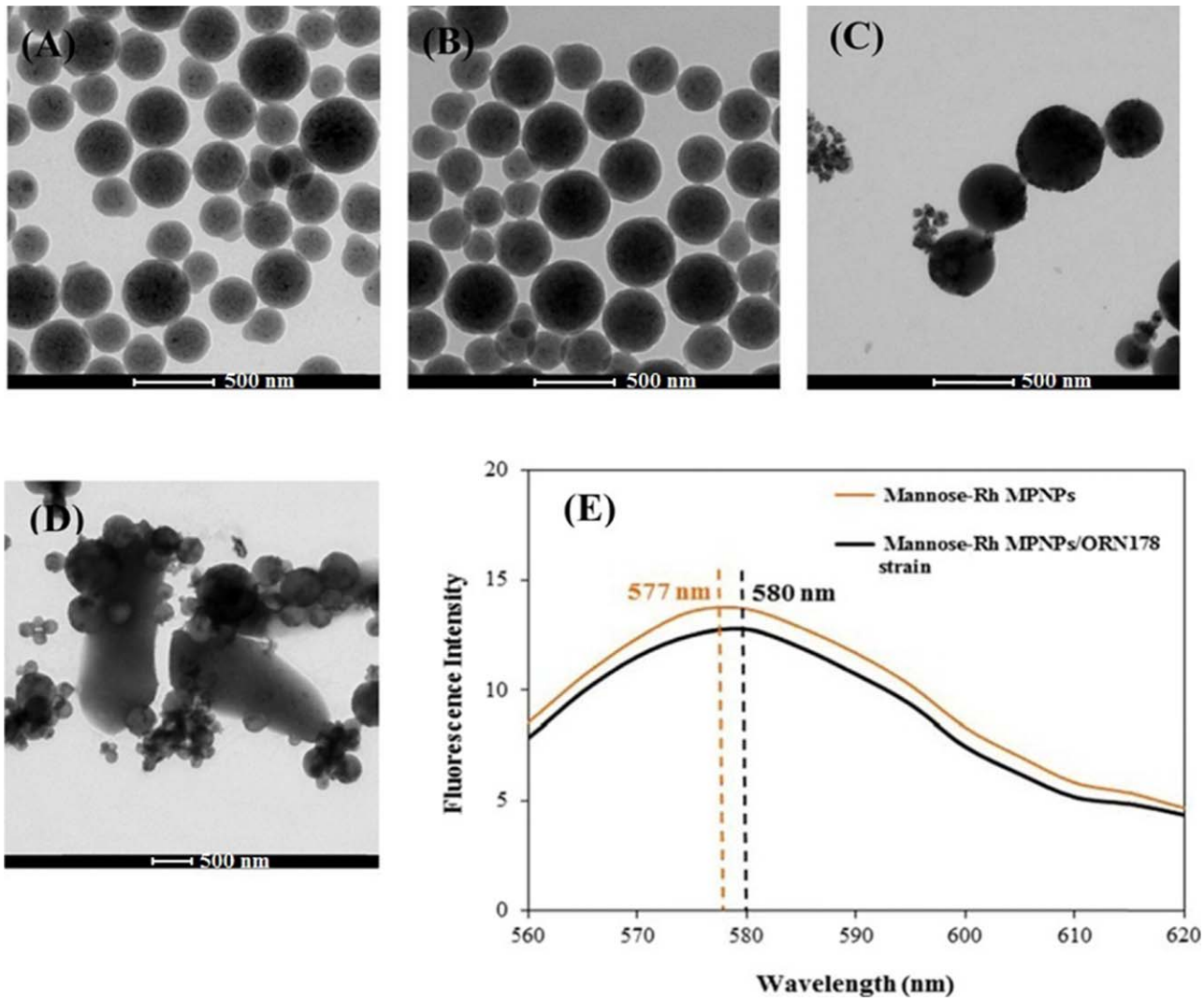

Figure 9. TEM micrographs of (A) MPNPs/ORN178 strain, (B) Rh B-MPNPs/ORN178 strain, (C) mannose-Rh MPNPs/ORN208 strain, (D) mannose-Rh MPNPs/ORN178 strain, and (E) fluorescence spectrum of mannose-Rh MPNPs/ORN178 strain when excited at 556 nm. [Color figure can be viewed in the online issue, which is available at wileyonlinelibrary.com.]

E. coli Detection

The mannose-Rh MPNPs were used for detection of two *E. coli* strains and binding between mannose-Rh MPNPs and *E. coli* cells was observed using TEM. The unmodified MPNPs were also incubated with ORN178 for use as a negative control. The TEM micrographs of MPNPs/ORN178, Rh B-MPNPs/ORN178, mannose-Rh MPNPs/ORN208 and mannose-Rh MPNPs/ORN178 are displayed in Figure 9(A–D), respectively. It should be noted that in Figure 9(A–C) only the MPNPs, Rh B-MPNPs, and mannose-Rh MPNPs were found due to the unbound bacteria, ORN178 and ORN208 strains, were discarded during the magnetic separation process. The fluorescence spectrum of the mannose-Rh MPNPs/ORN178 strain when excited at 556 nm is displayed in Figure 9(E).

As expected, the TEM image in Figure 9(A,B) demonstrate that the uncoated MPNPs and Rh B-MPNPs could not bind to the ORN178 strain, whereas the mannose-Rh MPNPs effectively attached to the ORN178 cells [Figure 9(D)]. This appeared to be due to specific binding of mannose on the mannose-Rh MPNPs to the FimH protein of *E. coli*.[12,35] It has been reported that all hydroxyl groups of mannose, except 1-OH, bind extensively with the FimH receptor. Residues within FimH make specific contacts with mannose including phenylalanine 1 (Phe1), asparagine 46 (Asn46), aspartic acid 47 (Asp47), aspartic acid 54 (Asp54), asparagine 135 (Asn135), glutamine 133 (Gln133), aspartic acid 140 (Asp140), and phenylalanine 142 (Phe142) that interact with mannose via hydrogen bonding and hydrophobic interactions. In addition, 2-OH of mannose interacts with water molecule inside FimH.[8,36] From Figure 9(D), it can be clearly observed that many mannose-Rh MPNPs are attached to each ORN178 *E. coli* cell. Additionally, the presence of several mannose molecules on each MPNP allowed for simultaneous multiple interactions of mannose-Rh MPNPs with the bacteria. This resulted in firm attachment of mannose-Rh MPNPs compared to monovalent binding.[35] The interaction of mannose-Rh MPNPs with *E. coli* required the FimH protein as no binding of MPNPs to strain ORN208 lacking the FimH protein was observed [Figure 9(C)]. After capture, the mannose-Rh MPNPs/*E. coli* complex could be rapidly and easily separated from the mixture by applying a magnet. Upon magnetic separation or washing, the multivalent interactions between the mannose-Rh MPNPs and *E. coli* cells were not disturbed and these multivalent interactions appeared to be critical for the mannose-based *E. coli* detection. The mannose-immobilized fluorescent polymer, mannosylated poly(*p*-phenylene ethylene) (PPE) contains several mannose units and could effectively bind to *E. coli* yielding brightly fluorescent aggregates of bacteria. In contrast, *E. coli* remained as individual cells after incubation with a mannose-functionalized fluorescent dye, 2′-fluorescein aminoethyl mannoside, that contains only one mannose unit and exhibits monovalent interactions with cells.[37]

The fluorescence property of the mannose-Rh MPNPs after binding to *E. coli* ORN178 was investigated using a microplate reader. As seen in Figure 9(E), the mannose-Rh MPNPs fluorescently labeled *E. coli* ORN178 resulting in a fluorescence emission peak at 580 nm. After binding, the emission of mannose-Rh MPNPs was red-shifted compared to that of the unbound mannose-Rh MPNPs (fluorescence emission peak at 577 nm). The slight shift in the emission peak might be due to an increase in π–π stacking interactions between the Rh B molecules as they were come into closer proximity when bound to bacteria.[37] Mannose-Rh MPNPs allows for a simple and rapid system for bacterial detection. Analysis time was 60 min (incubation of *E. coli* ORN178 and mannose-Rh MPNPs) which was much faster than the conventional culture techniques.

CONCLUSIONS

Mannose-Rh was successfully synthesized and immobilized onto PS/DVB/AA MPNPs. The high specific surface area of MPNPs allowed for the binding of 50 mg of mannose-Rh/g of MPNP. After incubating with *E. coli* ORN178 strain, several mannose-Rh MPNPs could bind to each *E. coli* cell resulting in fluorescently stained *E. coli* ORN178 with an emission peak at 580 nm. The mannose-Rh MPNPs have the potential for use as a simple and rapid *E. coli* detection system. This strategy also has the capacity to be expanded to exploit other carbohydrate–cell interactions for testing or labeling of disease causing pathogenic bacteria.

ACKNOWLEDGMENTS

This research work was supported by The Thailand Research Fund (TRF)/Commission on Higher Education (CHE) (RTA5480007). We thank Professor Paul Orndorff at North Carolina State University for kindly providing *E. coli* ORN178 and ORN208 strains.

REFERENCES

1. Ahmed, W.; Tucker, J.; Bettelheim, K. A.; Neller, R.; Katouli, M. *Water Res.* **2007**, *41*, 3785.
2. Abdel-Hamid, I.; Ivnitski, D.; Atanasov, P.; Wilkins, E. *Anal. Chim. Acta.* **1999**, *399*, 99.
3. Mittelmann, A. S.; Ron, E. Z.; Rishpon, J. *Anal. Chem.* **2002**, *74*, 903.
4. Ayçiçek, H.; Aydoğan, H.; Küçükkaraaslan, A.; Baysallar M.; Başustaoğlu, A. C. *Food Control.* **2004**, *15*, 253.
5. Taylor, A. D.; Ladd, J.; Yu, Q.; Chen, S.; Homola, J.; Jiang, S. *Biosens. Bioelectron.* **2006**, *22*, 752.
6. Lazcka, O.; Campo, F. J. D.; Muñoz, F. X. *Biosens. Bioelectron.* **2007**, *22*, 1205.
7. Velusamy, V.; Arshak, K.; Korostynska, O.; Oliwa, K.; Adley C. *Biotechnol. Adv.* **2010**, *28*, 232.
8. Sharon N. *BBA-Gen Subjects* **2006**, *1760*, 527.
9. Miller, E.; Garcia, T.; Hultgren, S.; Oberhauser, A. F. *Biophys. J.* **2006**, *91*, 3848.
10. Xue, C.; Jog, S. P.; Murthy, P.; Liu, H. *Biomacromolecules* **2006**, *7*, 2470.
11. Yang, W.; Pan, C.-Y.; Luo, M.-D.; Zhang, H.-B. *Biomacromolecules* **2010**, *11*, 1840.
12. El-Boubbou, K.; Gruden, C.; Huang, X. *J. Am. Chem. Soc.* **2007**, *129*, 13392.
13. El-Boubbou, K.; Huang, X. *Curr. Med. Chem.* **2011**, *18*, 2060.

14. Ge, Y.; Zhang, Y.; He, S.; Nie, F.; Teng, G.; Gu, N. *Nanoscale Res. Lett.* **2009**, *4*, 287.
15. Charoenmark, L.; Polpanich, D.; Thiramanas, R.; Tangboriboonrat, P. *Macromol. Res.* **2012**, *20*, 590.
16. Kaewsaneha, C.; Opaprakasit, P.; Polpanich, D.; Smanmoo S.; Tangboriboonrat, P. *J. Colloid Interface Sci.* **2012**, *377*, 145.
17. Lee, L. Y.; Ong, S. L.; Hu, J. Y.; Ng, W. J.; Feng, Y.; Tan, X.; Wong, S. W. *Appl. Environ. Microb.* **2004**, *70*, 5732.
18. Huo, F.-J.; Su, J.; Sun, Y.-Q.; Yin, C.-X.; Tong, H.-B.; Nie, Z.-X. *Dyes Pigments* **2010**, *86*, 50.
19. Zhang, X.; Shiraishi, Y.; Hirai, T. *Tetrahedron Lett.* **2007**, *48*, 5455.
20. Bhalla, V.; Tejpal, R.; Kumar, M. *Sensor Actuat. B-Chem.* **2010**, *151*, 180.
21. Gallagher, J. J.; Tekoriute, R.; O'Reilly, J.-A.; Kerskens, C.; Gun'ko, Y. K.; Lyncha, M. *J. Mater. Chem.* **2009**, *19*, 4081.
22. Lim, E.-K.; Yang, J.; Dinney, C. P. N.; Suh, J.-S.; Huh, Y.-M.; Haam, S. *Biomaterials* **2010**, *31*, 9310.
23. Yang, J.; Lim, E.-K.; Lee, H. J.; Park, J.; Lee, S. C.; Lee, K.; Yoon, H.-G.; Suh, J.-S.; Huh, Y.-M.; Haam, S. *Biomaterials* **2008**, *29*, 2548.
24. Liu, W.-Y.; Li, H.-Y.; Zhao, B.-X.; Miao, J.-Y. *Org. Biomol. Chem.* **2011**, *9*, 4802.
25. Luo, Y.-D.; Dai, C.-A.; Chiu, W.-Y. *J. Appl. Polym. Sci.* **2009**, *112*, 975.
26. Ohnishi, M.; Kozuka, Y.; Ye, Q.-L.; Yoshikawa, H.; Awaga, K.; Matsuno, R.; Kobayashi, M.; Takahara, A.; Yokoyama, T.; Bandow, S.; Iijima, S. *J. Mater. Chem.* **2006**, *16*, 3215.
27. Wan, J.; Yao, Y.; Tang, G. *Appl. Phys. A-Mater.* **2007**, *89*, 529.
28. Qiu, G.; Wang, Q.; Wang, C.; Lau, W.; Guo, Y. *Ultrason. Sonochem.* **2007**, *14*, 55.
29. Qian, Z.; Zhang, Z.; Chen, Y. *J. Colloid Interf. Sci.* **2008**, *327*, 354.
30. Brijmohan, S. B.; Swier, S.; Weiss, R. A.; Shaw, M. T. *Ind. Eng. Chem. Res.* **2005**, *44*, 8039.
31. Zhang, F.; Su, Z.; Wen, F.; Li, F. *Colloid Polym. Sci.* **2008**, *286*, 837.
32. Huang, J.; Pen, H.; Xu, Z.; Yi, C. *React. Funct. Polym.* **2008**, *68*, 332.
33. Polpanich, D.; Tangboriboonrat, P.; Elaïssari, A. *Colloid Polym. Sci.* **2005**, *284*, 183.
34. Heurtault, B.; Saulnier, P.; Pech, B.; Proust, J.-E.; Benoit, J.-P. *Biomaterials* **2003**, *24*, 4283.
35. Lin, C.-C.; Yeh, Y.-C.; Yang, C.-Y.; Chen, C.-L.; Chen, G.-F.; Chen, C.-C.; Wu, Y.-C. *J. Am. Chem. Soc.* **2002**, *124*, 3508.
36. Hung, C.-S.; Bouckaert, J.; Hung, D.; Pinkner, J.; Widberg, C.; DeFusco, A.; Auguste, C. G.; Strouse, R.; Langermann, S.; Waksman, G.; Hultgren, S. *J. Mol. Microbiol.* **2002**, *44*, 903.
37. Disney, M. D.; Zheng, J.; Swager, T. M.; Seeberger, P. H. *J. Am. Chem. Soc.* **2004**, *126*, 13343.